A review of recent results of mid-infrared quantum cascade photonic devices operating under external optical control

Olivier Spitz, Frédéric Grillot

JPhys Photonics

TOPICAL REVIEW • OPEN ACCESS

A review of recent results of mid-infrared quantum cascade photonic devices operating under external optical control

To cite this article: Olivier Spitz and Frédéric Grillot 2022 *J. Phys. Photonics* **4** 022001

IOP Publishing J. Phys. Photonics 4 (2022) 022001 https://doi.org/10.1088/2515-7647/ac5494

Journal of Physics: Photonics

OPEN ACCESS

RECEIVED
19 January 2021

REVISED
2 December 2021

ACCEPTED FOR PUBLICATION
11 February 2022

PUBLISHED
7 March 2022

TOPICAL REVIEW

A review of recent results of mid-infrared quantum cascade photonic devices operating under external optical control

Olivier Spitz[1,*] and **Frédéric Grillot**[1,2]

[1] LTCI, Télécom Paris, Institut Polytechnique de Paris, 19 place Marguerite Perey, 91120 Palaiseau, France
[2] Center for High Technology Materials, University of New Mexico, 1313 Goddard St. SE, Albuquerque, NM 87106-4343, United States of America
[*] Author to whom any correspondence should be addressed.

E-mail: olivier.spitz@telecom-paris.fr

Keywords: quantum cascade lasers, optical feedback, optical injection, non-linear dynamics, mid-infrared photonics

Abstract

The purpose of this article is to gather recent findings about the non-linear dynamics of distributed feedback quantum cascade lasers (QCLs), with a view on practical applications in a near future. As opposed to other semiconductor lasers, usually emitting in the visible or the near-infrared region, QCL technology takes advantage of intersubband transitions and quantum engineering to emit in the mid-infrared and far-infrared domain. This peculiarity and its physical consequences were long considered as a detrimental characteristic to generate non-linear dynamics under external optical control. However, we show that a wide diversity of phenomena, from high-dimensional chaos to giant pulses can be observed when the QCL is under external optical feedback or under optical injection and with a continuous current bias. Most of these phenomena have already been observed in other semiconductor lasers under optical feedback or under optical injection, which allows us to compare QCLs with their interband counterparts.

1. Introduction

The original interest in using external optical control techniques in semiconductor lasers is motivated by a desire to understand the associated limitations and instabilities and to develop strategies for controlling the underlying dynamics to improve the laser performance. Using these techniques, external optical perturbations can affect the parameters associated with the laser's dynamics, such as threshold gain, damping, spectral linewidth, intensity noise, and mode selectivity. The external optical perturbations can often produce undesired instabilities in the laser, but they can be well controlled to produce desirable laser properties, including improvement in the modulation characteristics and spectral stability.

The objective of this paper is to describe common external optical control techniques with the view on investigating their impact on the overall behavior of distributed feedback (DFB) quantum cascade lasers (QCLs), with a focus on the non-linear dynamics under external optical feedback (EOF) and optical injection. These techniques were previously studied thoroughly in bipolar lasers, but very little is known about the impact of external optical control on the performances of QCLs, including modulation characteristics and wavelength stability. QCLs are semiconductor lasers relying on inter-conduction-band quantum well transitions [1] and their emission domain ranges from the mid-infrared (mid-IR) to the terahertz (THz) region [2]. The topic of QCL has undergone fast development, with important breakthroughs still to be expected in the coming years [3–5]. The first operational device, working at cryogenic temperature and in pulsed mode, was produced at Bell Labs in 1994 after years of theoretical and technological improvements [6]. This was followed by continuous innovation since then, allowing QCLs to be operated at room temperature and with continuous-wave (CW) bias up to watts of output power over the 4–8 μm-range [7]. QCLs quickly replaced the other mid-IR sources that were previously available in civilian and defense sectors [8, 9]. QCLs are indeed candidates of choice for applications such as aerospace countermeasures [10], environmental and chemical gas sensing [11], free-space communication [12],

high-resolution spectroscopy and microscopy [13], breath analysis and other biomedical sensing [14]. In parallel, near-infrared semiconductor lasers have been thoroughly studied in the viewpoint of stability and dynamical properties since the beginning of the 90ies. As opposed to their near-infrared counterparts, studies about QCLs' non-linear dynamics in presence of optical feedback/injection are still sparse but are mandatory in order to fully unlock the potential of this mid-IR and THz sources. The goal of this paper is thus to review the recent advances of DFB-QCLs' non-linear dynamics when these lasers are either under optical feedback or under optical injection. We will also remind the predominant role of the linewidth-broadening factor (i.e. α-factor). This intrinsic parameter plays a key role in the behavior of other semiconductor lasers because it influences beam quality [15], filamentation [16], modulation properties [17] or inclination to non-linear phenomena. In that latter case, only lasers exhibiting a linewidth-broadening factor far above zero can display rich non-linear dynamics in a configuration with optical feedback. In QCLs, theory predicts a negligible linewidth-broadening factor because of the symmetric differential gain [18] but we will see that this is not in accordance with the experimental efforts about non-linear phenomena.

The paper shows that QCLs subject to optical feedback can generate chaos dynamics like low-frequency fluctuations (LFFs) and coherence-collapse regime which is highly meaningful for physical random bit generation. QCLs can also get locked under a master-slave optical injection configuration that is a key building-block toward the development of private communication based on chaos synchronization. Overall, we believe that this research work can also impact on the community of QCL interested in the dynamical properties of these lasers because they are related to various topics of greater interest such as mid-IR and THz frequency-combs, mode-locking and frequency stabilization. Besides, it is also of prime importance for researchers studying real-field applications of temporal chaos, as this work with QCLs opens up new possibilities in terms of private free-space communication and unpredictable countermeasure systems.

2. Linewidth-broadening factor

2.1. Origin and experimental determination

The linewidth-broadening factor is a parameter of paramount importance for studying the non-linear dynamics of QCLs that we will develop in the next sections. The α-factor drives the coupling between the phase and the amplitude of the electrical field or, in a similar manner, the coupling between the gain and the refractive index of the QCL [19]. This parameter that is typically involved in the dynamics of any semiconductor lasers is described as the ratio of the derivatives of the real and imaginary components of the first-order susceptibility $\chi^{(1)}$ with respect to the carrier density n [20]:

$$\alpha(\omega, n) = -\frac{\partial \chi_r^{(1)}(\omega, n)/\partial n}{\partial \chi_i^{(1)}(\omega, n)/\partial n}. \tag{1}$$

The operating point of the QCL determines the gain and the real part of the refractive index, that is to say $\chi_i^{(1)}$ and $\chi_r^{(1)}$ relatively independently of the excitation. Consequently, it implies a fixed value of n. When the injected current is suddenly modified, n, and therefore $\chi^{(1)}$, changes immediately. The process of returning to saturated values is very fast in QCLs thanks to ultrafast carrier dynamics whereby no relaxation oscillation involving the number of carriers and the energy of the field take place. Another peculiar definition of the α-factor, phenomenologically different, comes from the following equation [21]:

$$P = \varepsilon_0(\chi^{(1)} + \chi^{(3)}E^2)E \tag{2}$$

where P is the polarization, E is the electric field, ε_0 the vacuum permittivity, and $\chi^{(1)}$ and $\chi^{(3)}$ are the first two non-zero coefficients of the development of non-linear susceptibility. The imaginary part of $\chi^{(3)}$ accounts for the gain saturation whereas the real part corresponds to an intensity dependent optical index. Using this definition, the α-factor can be reformulated assuming the following equation:

$$\alpha = \frac{\chi_r^{(3)}}{\chi_i^{(3)}}. \tag{3}$$

This relationship was derived from a Van der Pol analysis of the laser noise taking into account the phase-amplitude coupling through an intensity-dependent index of refraction [22]. This is particularly relevant to analyze the phase-noise of QCLs and optical nonlinearities like spectral or spatial hole burning whereby the description of the non-linear susceptibility χ must incorporate an explicit dependence with $|E|^2$ [23]. Interestingly, when gain and optical index are instantaneous functions of intensity, the dynamics of the carriers are negligible and time constants associated with the saturation process can be neglected. In such a

way, equation (3) becomes identical to equation (1). However, when more complex dynamics of the carrier density are involved, like under rapid modulation, equation (3) cannot be used anymore. The α-factor is sometimes called linewidth-enhancement factor because the optical linewidth is magnified by a factor $(1+\alpha^2)$ compared to the Shawlow-Townes limit [24]. The linewidth of a semiconductor laser thus writes [25]:

$$\delta\nu = \frac{v_g^2 h\nu\,\alpha_{tot}\,\alpha_M\,n_{sp}}{4\pi P_0}\left(1+\alpha^2\right) \tag{4}$$

where v_g, n_{sp}, α_{tot}, α_M and P_0 are the group velocity, the spontaneous emission factor (or population inversion parameter), the total cavity losses, the mirror losses and the output power, respectively. If we define the full-width at half maximum (FWHM) of the cavity resonance as $\delta\nu_c = \frac{v_g\,\alpha_{tot}}{2\,\pi}$ and if we assume a lorentzian lineshape with a FWHM equal to 2γ for the intersubband transition, then the α-factor of a QCL is defined as a function of the center frequency of the gain spectrum ν_0 [1]:

$$\alpha(\nu) = \frac{\nu_0 - \nu}{\gamma} \tag{5}$$

and is thus close to zero because of an homogeneous gain medium. Indeed, both laser subbands of a QCL are within the conduction band and exhibit the same reciprocal space curvature. Equation (5) shows that α vanishes at the transition frequency, independently of n, hence characterizing detuned oscillators with $\nu \neq \nu_0$. It has to be noted that equation (5) can be applied to any laser that can be described by a two-level system (e.g. gas laser) and having an homogeneous broadening with lorentzian profile. Simulations of the α-factor in intersubband structures have shown the possibility for both negative and positive values, with a strong dependence on the carrier density [26].

Depending on whether the injection current is above or below threshold, different methods are considered to experimentally retrieve the α-factor for DFB-QCLs: the amplified spontaneous emission method [27] for current biases below threshold, the self-mixing interferometry [28] and high-frequency modulation [29] techniques to obtain α-factor for current biases above threshold. So far, experimental efforts in the mid-IR [30] and the THz domain [31] tend to confirm that the α-factor in QCLs is non-zero. In addition, although the first-order value of the QCL's α-factor is near-zero, any additional perturbation (e.g. thermal effects, spectral hole burning, etc) produces an increase of the effective α-factor which becomes most likely driven by the second-order terms, a situation well different than that in bipolar lasers. Last but not least, the various non-linear dynamics found in QCLs give credit to the hypothesis that QCLs exhibit α-factor between 1 and 2 because low α-factor values are not compatible with destabilization of semiconductor lasers [32]. The following sections aim at providing extensive details about destabilization and non-linear dynamics in QCLs, with a focus on experimental nonlinear dynamics in presence of optical feedback or injection.

2.2. Role of the linewidth-broadening factor for QCLs under EOF

The preponderant influence of the linewidth-broadening factor in the non-linear dynamics generated by QCLs subject to EOF can be understood with the Lang and Kobayashi model [33]. This model is widely used in numerical simulations for semiconductor lasers under self-feedback, and in the case of QCLs, this writes [34]:

$$\frac{dY}{ds} = (1+i\alpha)ZY + \eta e^{-i\Omega\theta}Y(s-\theta) \tag{6}$$

$$T\frac{dZ}{ds} = P - Z - (1+2Z)|Y|^2 \tag{7}$$

where Y and Z are the normalized complex electric field and the normalized carrier density, respectively, with the following definition:

$$Y = \sqrt{\frac{\tau_c G_N}{2}}E \tag{8}$$

$$Z = \left(\frac{\tau_p G_N}{2}\right)(N - N_{th}) \tag{9}$$

with τ_c the carrier lifetime, τ_p the photon lifetime, E the slowly varying envelop of the complex electric field, N the carrier density of the upper laser state, N_{th} the carrier density at threshold, G_N the differential gain, ω_0

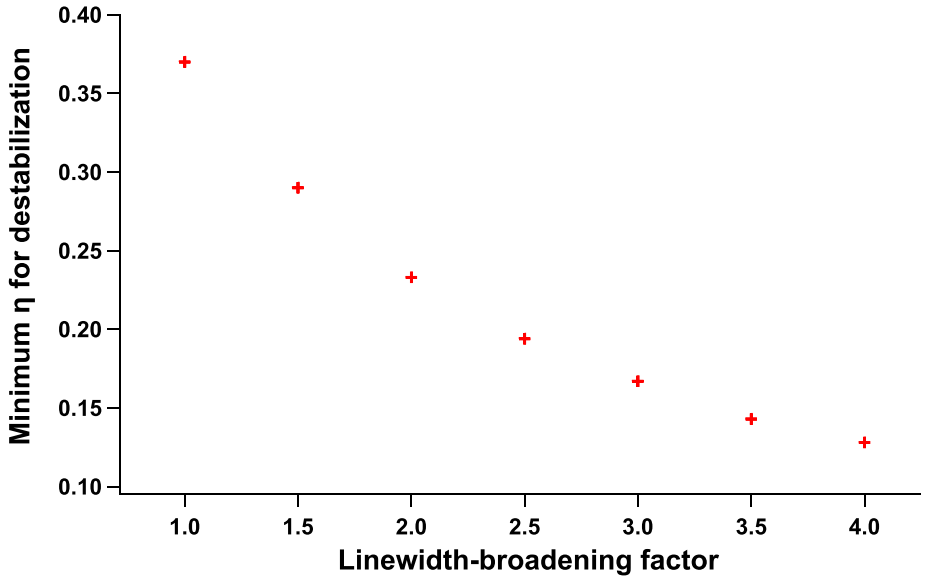

Figure 1. Minimum normalized feedback to observe a Hopf bifurcation in a QCL with EOF. The numerical model leading to this result is based on the Lang and Kobayashi model. Parameters used in this simulation are the same than those described in [32].

the free-running laser angular frequency, τ_{ext} the external-cavity round-trip time, k the feedback coefficient, $\eta = k\tau_p$ the normalized feedback ratio, $\Omega = \omega_0\ \tau_p$ the normalized free-running frequency, $\theta = \tau_{ext}/\tau_p$ the normalized external-cavity round-trip time, $T = \tau_c/\tau_p$ the carrier-to-photon lifetime ratio and P the pump parameter, defined as:

$$P = \frac{\tau_p G_N N_{th}}{2}\left(\frac{J}{J_{th}} - 1\right). \tag{10}$$

In equation (10), the threshold current J_{th} and the carrier density at threshold N_{th} are linked by $J_{th} = N_{th}q/\tau_c$ with q the electron charge. The feedback coefficient k is also defined by:

$$k = \frac{1}{\tau_{in}} 2\ C_l\sqrt{f_{ext}} \tag{11}$$

where f_{ext} is the ratio of the reflected power to the emitted power, τ_{in} the laser cavity roundtrip time and C_l the coupling strength coefficient at the front facet, whose expression is complex in DFB lasers and depends on facet phases as described in [35].

The linewidth-broadening factor is introduced in equation (6) and varying the value of this parameter changes the dynamical behavior of QCLs under EOF. More specifically, increasing the linewidth-broadening factor induces a reduction of the feedback ratio leading to the Hopf bifurcation, which corresponds to the first destabilization one can observe in such lasers. These numerical findings are summarized in figure 1 and the main conclusion is that for linewidth-broadening factor below 1, the Hopf bifurcation is not observed. This clearly confirms that this parameter cannot be negligible experimentally, because we are able to observe destabilization in QCLs under EOF, as shown hereafter.

3. QCLs with EOF

3.1. Laser destabilization

The model used to describe the dynamical behaviors of lasers was established by Haken in 1975 [36] in order to replace the previous hypothesis about noise-driven fluctuations in lasers emitting irregular trains of spikes [37]. The Haken model is ruled by a set of three equations, called the Lorenz-Haken equations [38], that reads:

$$\frac{dx(t)}{dt} = \sigma\big(y(t) - x(t)\big) \tag{12}$$

$$\frac{dy(t)}{dt} = -x(t)z(t) + rx(t) - (1 - i\delta)y(t) \tag{13}$$

$$\frac{dz(t)}{dt} = Re\left(x^*(t)y(t)\right) - bz(t). \tag{14}$$

In these differential equations, $x(t)$ is the time evolution of the scaled electric field, $y(t)$ is the atomic polarization and $z(t)$ is the population inversion. The parameter σ is the ratio of the decay rates for the population inversion ($\gamma_{\parallel}$) to that of the electric field (photons) from the laser cavity (κ_c). The parameters r and δ are the pump rate and the detuning of the atomic resonance frequency from the optical frequency. Finally, the parameter b is the ratio of the population inversion decay rate ($\gamma_{\parallel}$) to that of the atomic polarization ($\gamma_{\perp}$). Regarding the dynamics, lasers are classified in class A, B and C. Lasers with $\kappa_c \approx \gamma_{\perp} \approx \gamma_{\parallel}$ are called class C lasers [39]. The rate equations cannot be simplified in that case and the three differential equations are used to describe the dynamics. For instance, gas lasers such as NH_3 lasers and Ne-Xe lasers are Class C lasers. Mathematically, it is known from the Poincare–Bendixson theorem that at least three degrees of freedom, namely three independent variables, are required to observe deterministic chaos in continuous-time dynamical systems [40]. Therefore, only Class C lasers can produce instabilities under free-running operation. Lorenz–Haken chaos in a free-running laser was achieved in an 81.5 μm NH_3 laser, in which long wavelength and low pressure combine to achieve chaos conditions [41]. If one of these decay rates is larger than the others, the corresponding variable relaxes faster and consequently, it is possible to adiabatically eliminate some of the aforementioned equations while always keeping that for the electric field. When this elimination leads to two coupled equations, that is to say one for the population inversion and one for the electric field, the laser is considered Class B, for which $\gamma_{\perp} \gg \kappa_c > \gamma_{\parallel}$. Free-running Class B lasers are not prone to chaos dynamics because they require one extra degree of freedom to exhibit deterministic chaos. Yet, destabilization can occur through external perturbations. Among the most studied perturbations [42], one can cite external optical injection, modulation of the laser parameters, and various schemes of external optical or electro-optical feedback. One extra degree of freedom can also be achieved via Q-switching [43]. For instance, CO_2 lasers and laser diodes are Class B lasers. Thorough experimental and numerical details of laser chaos have been reported in a CO_2 laser where loss modulation provides the additional degree of freedom leading to non-linear dynamics [44]. Class B lasers are subject to relaxation oscillations, which means that the intensity response of the laser is not stable but produces a periodic signal, usually at several GHz. This property explains why all semiconductor lasers cannot be considered as Class B lasers. Indeed, some of them, such as QCLs, do not exhibit relaxation oscillations [45]. The last class of lasers requires two extra degrees of freedom in order to be destabilized and they are called Class A lasers for which $\gamma_{\perp} \approx \gamma_{\parallel} \gg \kappa_c$. In other words, the differential equations for population inversion and atomic polarization can be both eliminated. Consequently, these lasers are always very stable and dynamical effects do not easily occur. Examples of Class A lasers include, but are not limited to, visible He-Ne lasers and dye lasers.

3.2. Dynamical regimes

Following the discoveries of Haken, a rate equation model describing the standard dynamics of a single-mode semiconductor laser was introduced [46]. This was then complemented by the work of Lang and Kobayashi [33] to derive the formalism of a semiconductor laser under EOF (i.e. one of the configurations leading to non-linear phenomena), this model being restricted to the configuration where there is a single reflection on the feedback mirror, which is a fair approximation when the emitting facet reflectivity is not close to 1 (30% in our case). Experimentally, several dynamics have been spotted in many different semiconductor lasers: instability, bistability, self-pulsations, and coherence-collapse (CC) states [47]. It is relevant to note that EOF does not always lead to destabilization and is of utter interest for controlling the semiconductor laser properties. For instance, it is possible to tune and stabilize the linewidth of lasers by applying a strong optical feedback [48–51]. However, EOF can also have some downside effects in the case destabilization is the most dominant phenomenon, generally for high feedback strengths. These effects may disturb a transmission in the case where the external cavity is defined by the emitting facet of the laser diode and the input of the fiber. Usually, an isolation of 40 dB is mandatory to avoid reflection-sensitivity effects. Consequently, the dynamics of semiconductor lasers induced by EOF have a major impact on both real-field applications and fundamental studies [52].

Many parameters to characterize chaos and instabilities in semiconductor lasers exist, such as the α-factor, the bias current above threshold, the external-cavity length and the feedback strength. Previous works, like [34] extensively describe, with numerical simulations, the evolution of the bifurcation diagram of a QCL under EOF when varying these parameters. One of the most useful and most important parameters to give an accurate description of the non-linear phenomena is the feedback strength. The first investigation of semiconductor lasers with optical feedback was performed in 1986 [53]. The instabilities of semiconductor lasers with EOF are categorized into five regimes that are mainly connected to the feedback strength (which is

not straightforward to evaluate experimentally). However, the feedback strength is not the only ingredient since a phenomenon called restabilization sometimes occurs in semiconductor lasers under EOF and leads to an unpredictable repetition of the aforementioned regimes. These regimes, as well as the restabilization process, have been observed in almost every kind of semiconductor lasers, including highly-damped semiconductor lasers such as quantum dot lasers [54] and QCLs [34]. Along the discoveries, features have been added to the non-linear terminology to describe, for instance, sub-regimes of the CC [55] or to address the small-cavity regime [56], defined when $f_r\tau_{ext} < 1$, with f_r the relaxation oscillation frequency (if it exists) and τ_{ext} the external-cavity round-trip time. In the following, we will give more details about the configurations leading to chaos dynamics and that arise from the CC regime and the LFF regime.

3.2.1. LFFs, CC and chaos

The term CC was introduced by Lenstra and co-workers in 1985 [57]. Numerical simulations showed that, when the laser is subject to very high feedback ratios, the interaction between phase and amplitude induces linewidth enhancement [58] and a huge decrease of the coherence length compared to the free-running case. These findings were in good agreement with the experimental results. The relation between chaos and the CC regime was experimentally derived from the analysis of the RF spectrum of a laser, which was shown to match the power spectral density obtained with numerical simulations [59]. In addition, CC dynamics are generally characterized by a very broad RF spectrum whose limit frequency is often related to the intrinsic relaxation frequency in the case of the aforementioned near-infrared lasers. This observation initially supported the claim that QCLs may exhibit chaos waveforms with tremendously large RF bandwidths [60], but as we will see experimentally, the chaos bandwidth in QCLs seems to be limited by various complex parameters such as thermo-optical coupling within the quantum structure. That said, the lack of very high-speed (100 GHz) detectors in the mid-IR prevents from any definitive conclusion about both the absence of driving frequency and the limited bandwidth of non-linear dynamics.

LFFs is another kind of chaos fluctuations observed in lasers with EOF. LFFs were first reported for high feedback ratios close to the laser threshold, but it was later proved that LFFs can build-up for various conditions of operation. Indeed, because of the weak internal reflectivity of the front facet that characterizes many semiconductor lasers, LFFs are observed not only for currents near the solitary laser threshold, but also for larger injection currents [61]. Furthermore, increasing the injection current leads to LFFs with higher frequency components [62]. LFFs were primarily viewed as an obstacle to high-precision applications because they induce more fluctuations compared with the free-running case. LFFs are characterized by a sudden power dropout with a following gradual power recovery, or sometimes reciprocally for QCLs under EOF, as we will see in the experimental section. The LFF pattern is composed of irregular pulses but three frequency components are predominant. The main repetition frequency of LFFs is usually in the order of a few MHz to a few dozens of MHz. The name LFFs actually comes from this component that is rather slow compared to the dynamics of other forms of chaos. Indeed, in other semiconductor lasers, chaos fluctuations are connected to the relaxation oscillations of the laser (if any), and the frequency of these oscillations is often at several GHz [63]. LFFs also contain the signature of the external-cavity length, as we will see in the next section, and another faster time structure within the waveform, consisting of series of subnanosecond pulses that can be experimentally observed with a streak camera [64].

A method exists to characterize this kind of deterministic chaos and it is based on the study of the statistics of the period between two consecutive drop-outs [65, 66]. In the case of a QCL under EOF, this statistics shows a characteristic death area, which represents a period of roughly $10 \times \tau_{ext}$ below which no upcoming event is triggered [67]. Moreover, the statistical distribution has the shape of a decaying exponential at low injection current, and a second maximum pops up for stronger injection currents. With the help of such distribution, it is possible to distinguish LFF timetraces from other spiking phenomena.

3.2.2. Experimental results

After the discoveries related to deterministic chaos for several semiconductor lasers in the 80ies and the 90ies [68–71], it was relevant to extend these notions to QCLs because their emission wavelengths in the mid-IR make them useful for several applications [72–74] which cannot be addressed with near-infrared and visible-light semiconductor lasers. However, QCLs do not exhibit relaxation oscillations [75] and they are renown for their low α-factor compared to other semiconductor lasers [76, 77] which, overall, brings stability to QCLs subject to external perturbations. It is thus not surprising that some experimental configurations led to stability of QCLs against optical feedback [51, 78]. Several methods exist to trigger chaos in the output of a laser and we will focus on chaos obtained with EOF, as illustrated in figure 2. The first experimental proof of LFFs in QCLs was given by Jumpertz and co-workers in 2016 [67]. At both near-threshold pump current and high feedback strength, they were able to follow the evolution of the non-linear dynamics, with the advent of oscillations at the frequency of the external cavity and then, at

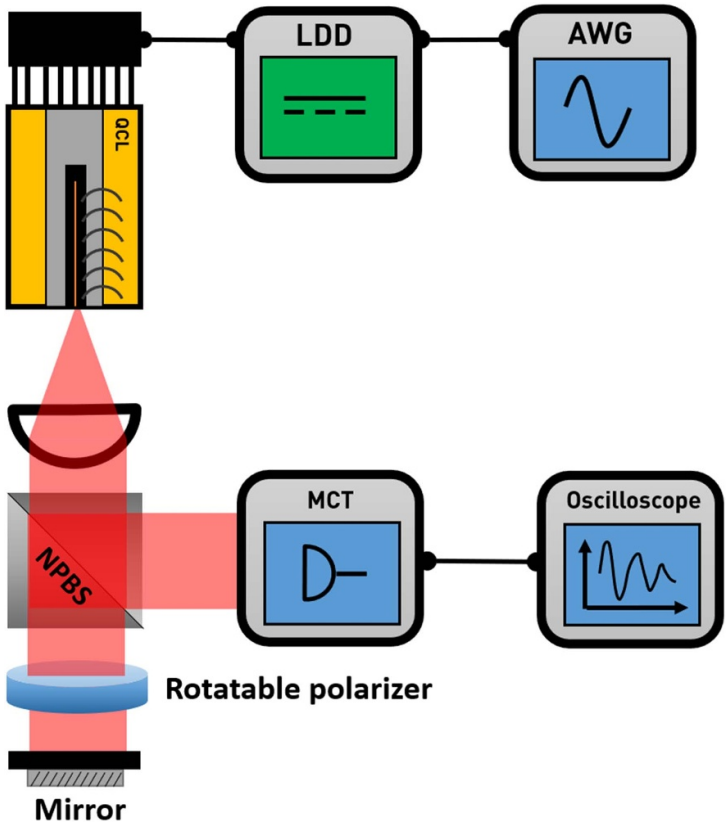

Figure 2. Experimental setup with an external cavity for the optical feedback provided by a gold-plated mirror; NBPS: non-polarizing beam splitter, MCT: Mercury-Cadmium-Telluride detector, AWG: arbitrary waveform generator, LDD: laser diode driver.

higher feedback strength, LFFs containing both the frequency of the external cavity and the dropout signature. Not only they exhibited the temporal chaos waveforms, but also they performed thorough numerical simulations based on the Lang and Kobayashi equations already mentioned. When taking into account the peculiarities of QCLs, namely a low α-factor and a very low carrier-to-photon lifetime, the simulations showed a Hopf bifurcation followed by a chaos bubble, and were compatible with the experimental results. Although of prime importance because it was the first proof-of-concept of chaos in mid-IR DFB-QCLs, these preliminary results left many questions unanswered. The non-linear dynamics were observed only close to the threshold current for a quasi-continuous bias and at room temperature. In order to have a comprehensive overview of the phenomenon and to take advantage of it for applications, it was necessary to determine if non-linear dynamics can also be observed far from threshold current and with continuous bias. Indeed, these two conditions will favor the use of QCLs' non-linear dynamics for applications like chaos private free-space communication [79] and physical random number generation [80]. As already described in [81], it is possible to experimentally exhibit dynamics restabilization in the case of QCLs under EOF. This means that stable signal or chaos islands can be found several times in a bifurcation diagram. Overall, the observation of a given non-linear phenomenon for a given feedback strength mainly depends on the initial conditions in the case of a CW bias. This peculiarity of chaos dynamics, as well as the wide diversity of bifurcation diagrams one can observe with the same QCL, is in favor of a general description of the exhibited non-linear phenomena rather than an extensive description of the experimental parameters (external cavity length, feedback strength, bias current…) leading to a given phenomenon. However, the general trend is that it is easier to observe robust and reproducible non-linear dynamics when one reduces the external cavity length, powers the QCL far above threshold current and performs very slow and accurate feedback strength modifications, for instance with a polarizer on piezo-electric actuators.

In the following, we will describe the conventional non-linear dynamics that we were able to observe with our DFB-QCL in an external-cavity configuration. External-cavity frequency oscillations, period-doubling oscillations, LFFs and CC dynamics can be visualized in figures 3–5. They are generally observed in that order, for an increasing value of the feedback strength but, as aforementioned, restabilizations can alter such order. The main characteristic of these dynamics is that they contain the frequency of the external cavity and then, more or less complex features. In the case of oscillations at the external-cavity frequency, no other

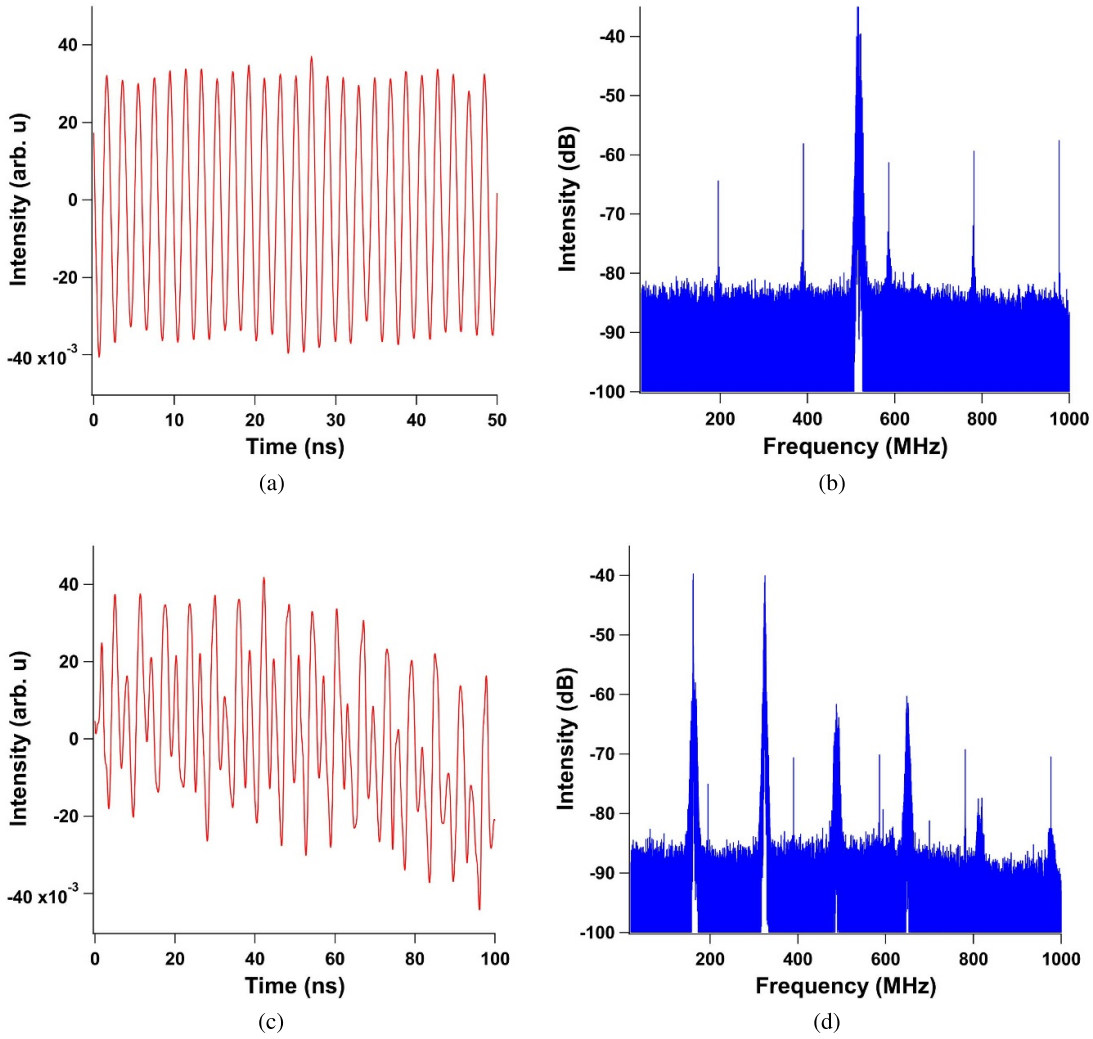

Figure 3. Experimental time traces of the output of the QCL when it exhibits non-linear dynamics that are not chaotic (left panels). RF spectrum analysis of the signal (right panels). (a), (b) Correspond to the case of oscillations at the external-cavity frequency; (c), (d) correspond to a period-doubling phenomenon.

feature is spotted and the time trace is a regular sine wave (figure 3(a)). When the length of the external cavity is 25 cm, the related external-cavity frequency should be 600 MHz but experimentally, the retrieved frequency is always a bit lower, as shown in figure 3(b) where the peak RF frequency is measured around 520 MHz. This discrepancy has already been reported in QCLs [82]. More complex dynamics are likely to be generated by the QCL. Period-doubling corresponds to a configuration where the frequency of the external cavity is clearly seen but is modulated by another periodic signal, as shown in figure 3(c). The related RF spectrum (figure 3(d)) is composed of a combination of frequencies related to the external-cavity period and twice the external-cavity period, which explains the designation period-doubling phenomenon. In our case, the observed frequencies are 162.5, 325, 487.5, 650, 812.5 and 975 MHz (i.e. integer multiples of 162.5 MHz). The highest frequencies are more difficult to observe due to the 3-dB cutoff frequency of the MCT detector around 700 MHz. The two non-linear dynamics we just mentioned are not chaos phenomena. The chaos nature of such signal can be further analyzed with Lyapunov exponents [82] which will not be described in this article.

Transition toward a chaotic behavior occurs when LFF are observed (figure 4(a)). The LFF pattern in QCLs has a maximum frequency of a few dozens of MHz with a wide low-frequency component, as shown in figure 4(b), but the contribution of the external cavity at several hundreds of MHz is still present and can be observed by carefully zooming on the LFF signal, for instance in figures 4(c) and (d). LFF is a phenomenon that is also observed in other semiconductor lasers subject to EOF, such as laser diodes, but in the case of near-infrared lasers, the shape of the LFF is usually reversed. The other chaos phenomenon one can observe with QCLs is CC dynamics and is of paramount importance for private communication with chaos or physical random bit generation because it corresponds to highly complex patterns, designated as hyperchaos

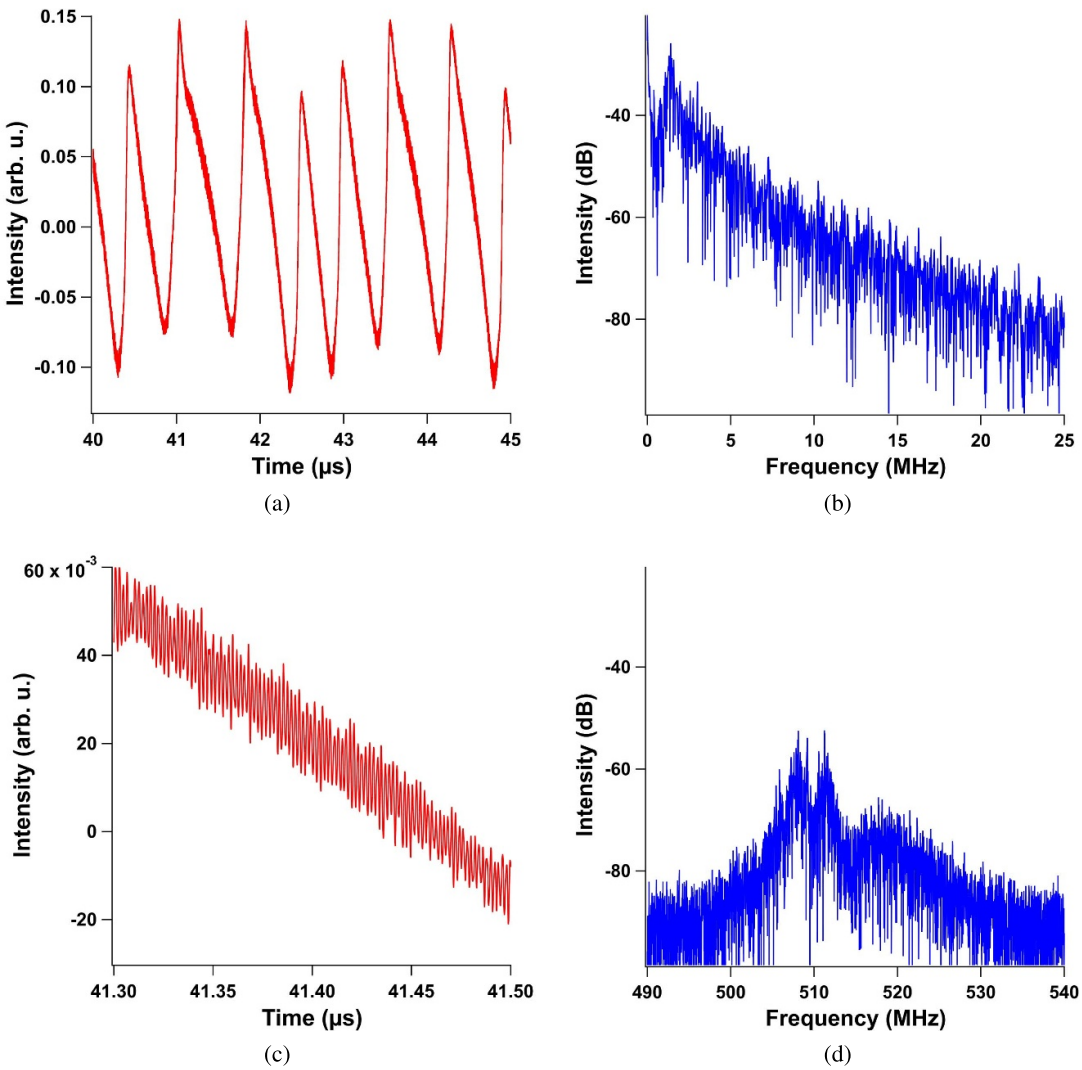

Figure 4. Experimental time traces of the output of the QCL when it exhibits LFF dynamics (left panels). RF spectrum analysis of the signal (right panels). (a), (b) Correspond to the global LFF pattern; (c), (d) correspond to a zoom of the observed dynamics and allow retrieving the signature of the external-cavity frequency.

when more than one Lyapunov exponent can be retrieved [83]. A typical example of CC dynamics in DFB-QCL under EOF is shown in figure 5(a). Again, the RF spectrum of the chaos component spreads out but is limited to 25 MHz in figure 5(b) (contrary to what can be found in near-infrared lasers) and a closer look at the signal allows retrieving the external-cavity frequency in figures 5(c) and (d). Something that is relevant to note is that destabilization in QCLs arises from the external-cavity frequency, and this is the reason why this frequency can be found in the RF spectrum for the dynamics we described. In other semiconductor lasers, which are categorized as Class B lasers, destabilization is related to the relaxation frequency (generally in the order of a few GHz). This configuration cannot apply to QCLs because they do not exhibit relaxation oscillations as they are overdamped semiconductor lasers.

3.3. Other QCLs and feedback configurations

In the previous subsection, we have only focused on DFB-QCLs, and investigations considering other QCL configurations can be found in the literature [78, 84]. We have described typical non-linear dynamics that can be observed with EOF, sometimes called conventional optical feedback, because this configuration corresponds to the reinjection of the light back to the QCL with a regular mirror. This means that the mid-IR light is not altered on its way back to the laser's cavity. Other optical feedback configurations exist but will not be fully detailed in this work. One can cite phase-conjugate feedback where the reinjected beam is self-correcting and self-aligning [85]. That describes the principle that any phase-shift and spreading that the laser beam could undergo in its path from the emitting facet of the semiconductor laser to the mirror due to propagation in the air or through distorting media is compensated in the backward trip. This means that,

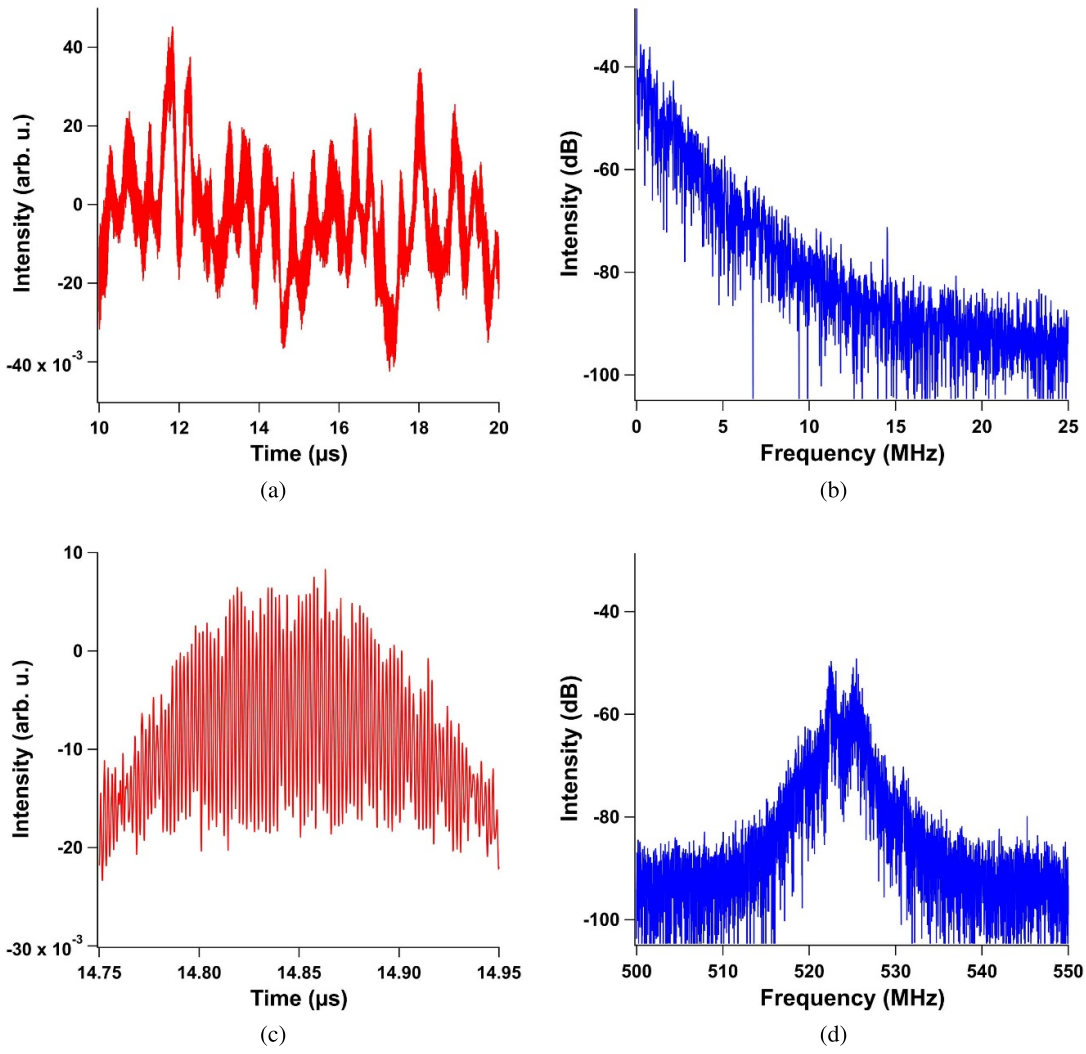

Figure 5. Experimental time traces of the output of the QCL when it exhibits CC dynamics (left panels). RF spectrum analysis of the signal (right panels). (a), (b) Correspond to the global CC pattern; (c), (d) correspond to a zoom of the observed dynamics and allow retrieving the signature of the external-cavity frequency.

when fed back into the laser cavity, the photons have exactly the same phase as at the moment they were emitted out of it. Actually, phase conjugation is an equivalent of the time-reversal phenomenon [86], which is not limited to the optoelectronics domain [87, 88]. This technique is however more difficult to implement because it relies on four-wave mixing process and this is generally achieved when the beam from the semiconductor laser is sent toward a grating and the resulting scattering on the grating creates a fourth beam which properties are to be counter-propagating and phase-conjugate with respect to the initial beam [89]. This complex implementation has hindered experimental efforts with QCLs under phase-conjugate feedback but it is relevant to note that a few numerical studies are available [90]. Another example that differs from conventional optical feedback is what is broadly called cross-polarization feedback. In this configuration, the polarization of the feedback light is rotated on its way back to the laser cavity. This technique has been used in semiconductor lasers that emit on two orthogonal polarizations, such as vertical-cavity surface-emitting lasers [91], but also in semiconductor lasers where one of the two polarization states is mostly suppressed. For instance in laser diodes, the TM mode is mainly suppressed but a cross-polarization feedback scheme was proven useful in generating dynamics in this otherwise suppressed TM mode [92]. The most relevant option to implement a cross-polarization configuration is to insert a Faraday rotator within a linear external cavity [93], because this allows selecting a single, linear polarization state for the light that is fed back, which simplifies interpretation of the observed non-linear phenomena. Another possibility to select a single polarization state relies on a loop-injection scheme with an optical isolator, a half-wave plate and a polarizer [94]. The last method consists in inserting a quarter-wave plate within the linear external cavity. If the output

light is perfectly TM polarized (as it is almost the case in QCLs), the polarization of the wave will become circular after the first crossing through the quarter-wave plate. Then, the wave is reflected by the mirror, so the polarization remains circular but in the opposite direction. On its way back to the laser, this circularly polarized wave travels once again through the quarter-wave plate, which converts it into a TE wave. Consequently, this method allows turning a linearly polarized wave into a linear orthogonal wave. However, if the initial wave is not purely linear, the feedback wave will have a polarization state more complex than the one previously described, and it is difficult to control what is the exact amount of TM/TE polarization reinjected into the laser. This third method has been recently investigated in the case of mid-IR QCLs [95] but the theory is still lacking to explain the experimental findings.

4. Giant pulses in QCLs with tilted EOF

4.1. Giant pulses in optics

Following the efforts about giant waves in an oceanographic context [96, 97], the concept of extreme events (which encompasses rogue events) was extended to many research fields, such as economics [98], acoustics [99] and astrophysics [100], with similar properties but sometimes different mechanisms. In hydrodynamics, this term is applied for single waves that are extremely unlikely as judged by the Rayleigh distribution of wave heights [101]. In optics, giant pulses were first mentioned in 2007 in the context of super-continuum generation in optical fibers at a near-infrared wavelength [102]. In this first demonstration, giant pulses were categorized as rogue events because their occurrence was theoretically explained by a generalized Non-Linear Schrödinger equation, which confirmed not only the mechanism for giant pulses but also the soliton behavior that was previously found in hydrodynamics systems [103]. This discovery paved the way for the analysis of giant events in many other domains of physics and continues to inspire innovative advances [104].

In semiconductor lasers, the first experimental demonstration of giant pulses was released in 2011 [105] and the rare occurrence of these high-amplitude pulses was confirmed by simulations based on a simple noise-free rate equation model compatible with a deterministic non-linear process. Most of the experimental and numerical works studying giant pulses in semiconductor lasers focus on an injection scheme [106–108]. VCSELs and laser diodes are the most common devices in these experiments because they are renowned for their sensitivity to external perturbations. A very limited number of papers deals with the study of giant pulses in the case of optical feedback [109, 110] and, among these papers, the conventional optical feedback is sometimes replaced by phase-conjugate feedback [111] or filtered optical feedback [112]. Without any specific control, giant pulses are expected to pop up randomly and may not be reliable for applications. Yet, extensive studies about controllable giant pulses can be found in the literature [113–116] with the view of taking advantage of these sudden bursts for high precision remote-sensing [117] or photonic reservoir computing [118].

4.2. Giant pulses in QCLs

As we will expose in the following, giant pulses can be triggered in a QCL under EOF, and more specifically when a pulse-up pattern is applied to the electrical bias of the laser. Hence, it is of first importance to study and map this phenomenon because it can really disturb the message encoded via the electrical current of the QCL when it comes to realize a private free-space transmission [79]. The succession of bits can indeed be considered as a pulse-up and if giant pulses pop up, they can magnify the hidden bits and reveal them in the viewpoint of an eavesdropper. In order to generate giant pulses with a QCL under EOF, we consider the same setup than that described in figure 2, except that the feedback mirror is slightly tilted and the reinjected light may couple with lateral modes if the laser cavity is wide enough. Recent work by another group has shown that it is also possible to trigger non-linear dynamics, like those shown previously, with this tilt configuration [119]. Figure 6(a) shows a typical timetrace gathering giant pulses with an amplitude larger than several times the standard deviation of the free-running signal. A peculiar feature of these pulses is that their amplitude varies and there is a continuous distribution of the events heights. This basically means that the amplitude of the upcoming giant pulse is unpredictable. Figure 6(b) shows that the time-interval between the events we observed is not easily foreseen, which is another characteristic of giant pulses. Other studies have shown that the separation time (S) between giant events follows a Poissonian distribution [120] when the time elapsed between these events (numbered $k-1$ and k) is written in log scale: $S = \log(T_k) - \log(T_{k-1})$. A deviation of the statistics is sometimes found for high feedback ratios [121], and in this case, the curve is characterized by two slopes instead of one. Figure 6(b) shows the evolution of the separation count with S when taking into account 419 giant pulses intervals in the case of a QCL. The trend follows a decreasing exponential as encountered in other semiconductor lasers.

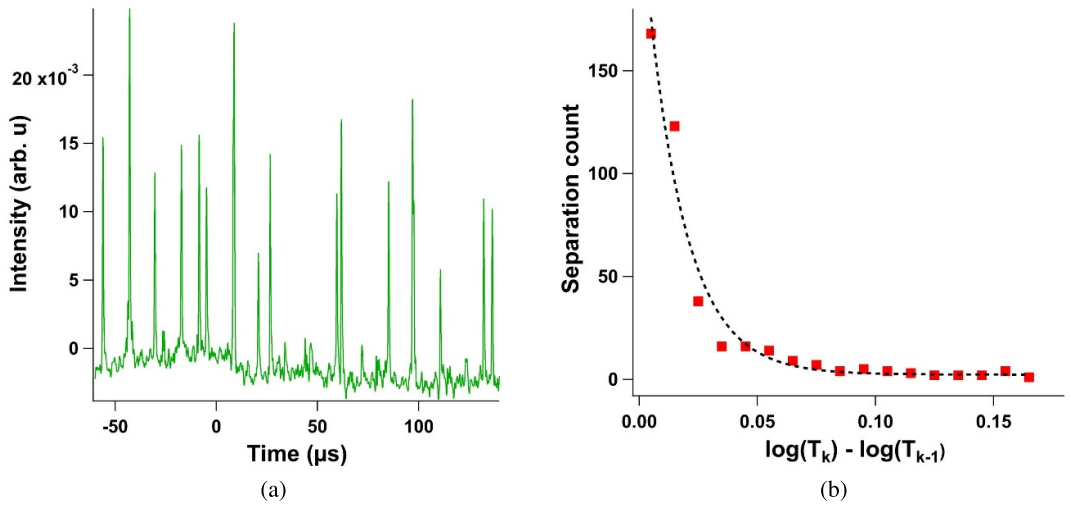

Figure 6. (a) Experimental time trace of the output of the QCL showing giant pulses randomly triggered in time and with various amplitudes. (b) Statistical distribution of the log-scale time intervals between giant pulses with its decaying-exponential fit (black dashed curve).

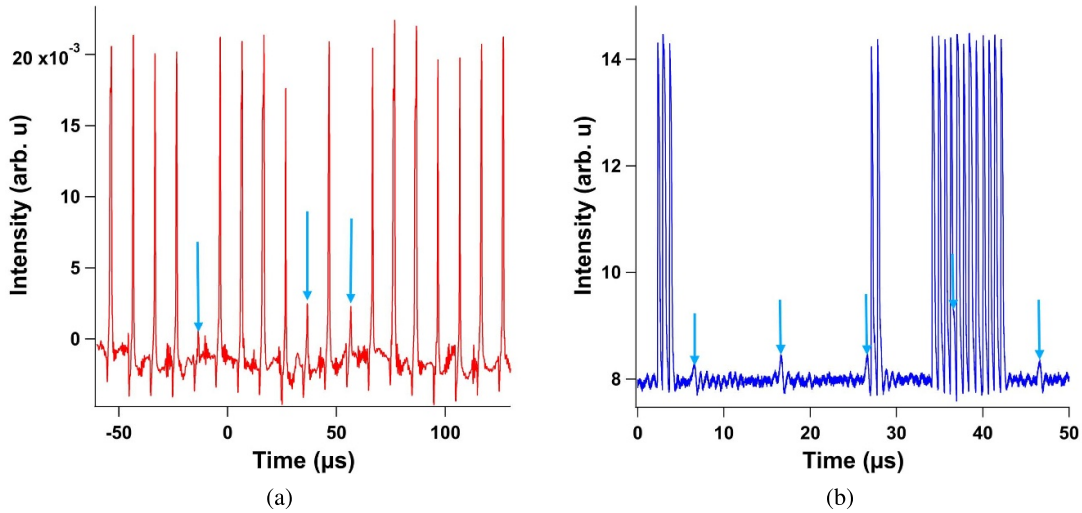

Figure 7. (a) Experimental time trace of the output of the QCL when adding a periodic electrical excitation. The success for triggering giant pulses is high and only a few excitation signals do not give birth to extreme events (light blue arrows). For the triggered giant pulses, they are synchronized with excitation and their amplitude is consistent. (b) Configuration where the amplitude of the pulse-up excitation (light blue arrows) is not sufficient to trigger synchronized giant pulses; trains of consistent pulses are yet fired in a time-irregular pattern.

It is possible to tune the time intervals between the giant pulses and to stabilize their amplitude by adding a periodic electrical perturbation. Figure 7(a) shows giant pulses with a consistent amplitude and they are synchronized with the small pulse-up signal at a repetition frequency of 100 kHz. This electrical pulse-up signal generally triggers a giant pulse in the optical response but the success rate is not 100%. The small excitation pulses which were not followed by a giant pulse are marked with light blue arrows in figure 7(a). However, the parameters of the pulse-up excitation must be chosen carefully, otherwise the triggering process is noneffective. Figure 7(b) shows another example where the repetition frequency of the excitation signal is 100 kHz but with a lower amplitude. The resulting optical response is a train of giant pulses with a very homogeneous amplitude but they are not synchronized with the pulse-up excitation (marked with light blue arrows). Furthermore, the number of giant pulses within each bursting train seems to be random and no specific relation between two consecutive trains can be drawn. It is relevant to note that the two configurations we just described have a time distribution which does not match the regular giant pulses distributions because of the extra electrical excitation disturbing the non-linear process.

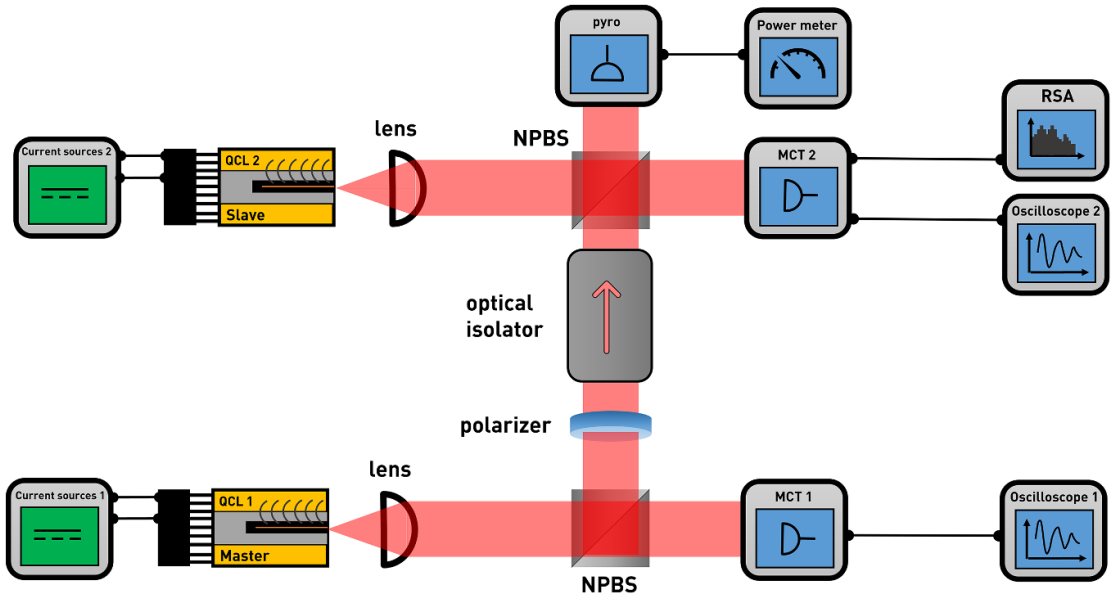

Figure 8. Setup for the optical injection of a free-running master laser into a slave laser. A polarizer allows varying the optical injection strength while the optical isolator avoids back-injection from the slave laser. NPBS: non-polarizing beam splitter; MCT: Mercury-Cadmium-Telluride detector; pyro: pyro-electric detector; RSA: electrical spectrum analyzer.

5. QCLs with optical injection

5.1. Configuration with free-running QCLs

In optical injection, the light of a master laser is sent toward the cavity of a slave laser. As we will see in the following, the master laser may be free-running or may exhibit non-linear dynamics before being injected into the slave laser. In the optical injection experimental setup shown in figure 8, avoiding optical feedback in the master laser after reflection on the slave's facet is of paramount importance, as well as avoiding optical injection from the slave laser toward the master laser, and this is the reason why an optical isolator is placed between the two lasers. Without optical isolator, the two lasers impact each other, and this corresponds to mutually coupled lasers, which also experience complex dynamics [122]. We tested a mutual coupling scheme in the case of QCLs and saw that, even when the coupling between the two lasers is weak, the slave QCL can really disturb the non-linear pattern of the master QCL, hence justifying the necessity of an optical isolator between the two lasers. This is illustrated by figure 9. Optical injection can improve the emission properties of the slave laser with a significant impact. In the case of injection-locking, the emission properties of the slave laser are changed. For instance, the side-modes of a Fabry–Perot (FP) slave laser can be suppressed [123] while the spectral linewidth of the slave laser can be reduced by one order of magnitude [124]. Other improvements have been studied in semiconductor lasers, both numerically and experimentally, in terms of intensity-noise, frequency-noise and bandwidth. If the master laser has low intensity-noise and phase-noise, then the slave laser tends to reproduce the intensity-noise and frequency-noise of the master [125]. In laser diodes, optical injection was also found useful in enhancing the chaos bandwidth of a slave laser subsequently subject to EOF [126]. This technique is also very relevant in terms of private communication if a third laser is used for the synchronization of the enhanced chaos [127].

Taubman and co-workers reported the first injection-locking of a DFB-QCL into another DFB-QCL [128]. When increasing the injection strength up to 3%, they observed a locking range of $\pm$500 MHz. The second key observation was a strong optical linewidth reduction in the slave laser and this was deduced by observing the heterodyne beating between the slave QCL and the master QCL. Noise limitations have also been tackled with the help of optical injection-locking. In particular, when injecting a DFB-QCL into a second DFB-QCL, numerical simulations showed a 20 dB Hz^{-1} reduction of the relative intensity noise (RIN) at low frequency [129]. The experiments following the numerical efforts achieved a 10 dB Hz^{-1} reduction of the RIN [130]. In a DFB-QCL, the optical side modes are suppressed by the grating to achieve single-mode emission. But in the case of optical injection, the optical frequency of the master can quench the main mode of the free-running slave QCL to enhance, one after another, the side-modes of the slave. This phenomenon comes with RIN reduction and optical power increase. By injecting a frequency-comb into a FP-QCL, the low-frequency noise was also significantly reduced [131]. The global idea when studying optical

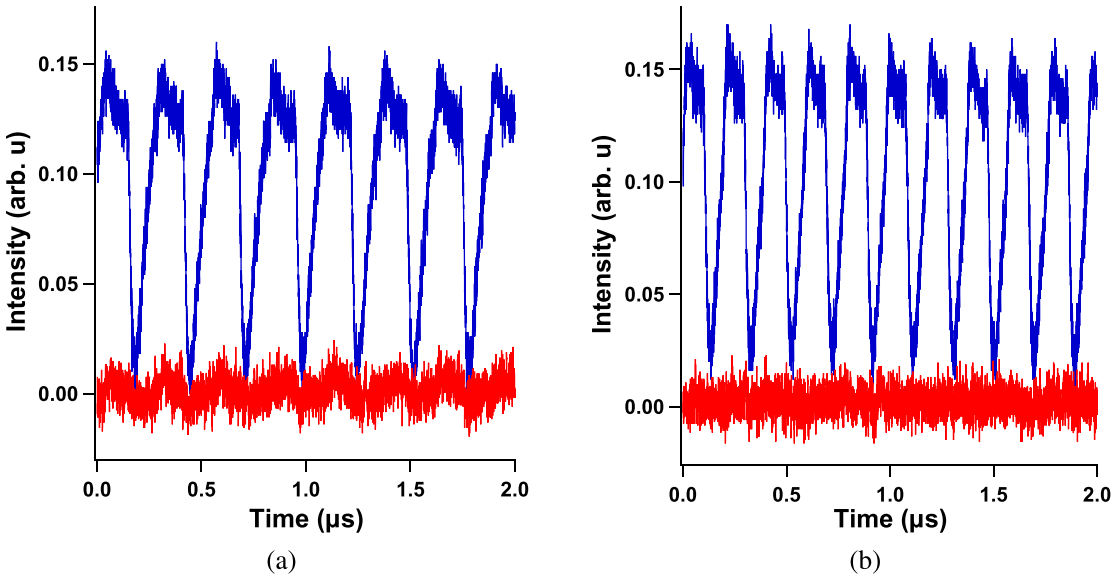

Figure 9. (a) The master laser (in blue) is driven chaotic and is weakly coupled into the slave laser (in red) which weakly synchronizes with the fluctuations of the master. There is no optical isolator between them, so the slave laser influences in turns the master output. (b) When hiding the path between the two lasers, the synchronization is (obviously) lost but the frequencies of the master non-linear fluctuations are also modified. This highlights the fact that an optical isolator is required between the two lasers, otherwise the slave can disturb the master laser, even if they are weakly coupled.

injection is that the master's behavior is reproduced by the slave QCL, and the best performance were achieved by reducing the frequency noise of the slave by several orders of magnitude or decreasing the optical linewidth of the slave to 20 kHz while the free-running slave laser had a linewidth of several MHz.

Another interest of optical injection in QCLs is to improve the modulation bandwidth of such lasers. In their near-infrared counterparts, it was shown experimentally that a high injection rate (up to 45% of the slave output intensity) drastically enhances the bandwidth of the slave laser [132]. Based on QCL rate equations, a few theoretical efforts [133, 134] showed an increase of the modulation bandwidth of several dozens of GHz. Apart from showing the improved modulation bandwidth, these theoretical efforts found no unstable locking region in the injected QCL, provided that the frequency detuning remains small [135]. A potential explanation for this relies on the ultra-fast carrier lifetime in such gain medium. Yet, these predictions are not supported by experimental studies and we will see in the following that injected QCLs can be destabilized, even though the optical detuning between the master and the slave laser is small.

5.2. Experimental results with QCLs

The numerical model for the non-linear dynamics analysis of a QCL under optical injection was developed by Erneux and co-workers [136] and then subsequently studied in [34]. Depending on the injection rate and the detuning between the master QCL and the slave QCL, the latter exhibits damped oscillations, overdamped oscillations or a pattern looking like the one found in LFFs, but with a more periodic repetition rate. Another finding from the numerical efforts is that the repetition rate of the oscillations (if any) is dependent on the injection rate and its frequency is, at maximum, the value of the optical detuning between the master and the slave.

When injecting unidirectionally the light of a free-running master QCL into a free-running slave QCL, the slave is destabilized and its optical output is no longer constant, provided that the optical detuning between the two lasers is small. Typical dynamics generated by the slave can be seen in figure 10(a) (red trace) and the non-linear phenomenon observed looks similar to the one retrieved with a numerical simulation based on the aforementioned model and shown in figure 10(b). In both cases, the dynamics show a LFF-like pattern with the main frequency centered around the value of the frequency detuning for the experimental results and a main frequency lower than the frequency detuning for the numerical result. The main difference between the simulation and the experimental work is that changing the injection strength does not modify the frequency of the observed pattern in the experimental case. Indeed, the only parameter affecting the slave output is the optical frequency detuning between the master and the slave, as illustrated in figure 11. When the optical detuning between the master and the slave QCL is too large, it is not possible to observe the aforementioned dynamics and the slave output is only noisy, as shown in figure 10(a) (blue trace). The value of the frequency detuning is actually the main frequency component of the RF spectrum

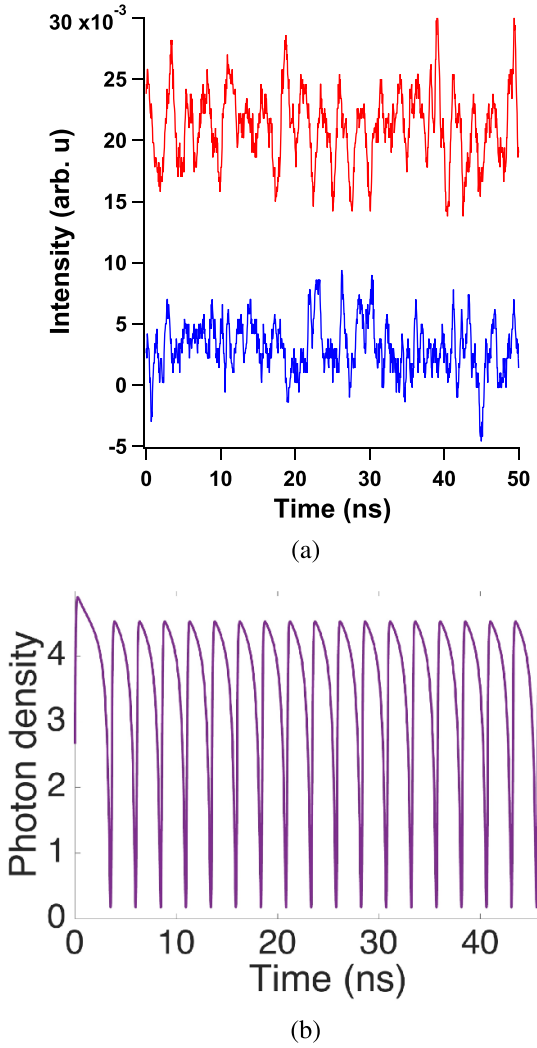

Figure 10. (a) Experimental time traces of the output of the slave QCL when the bias current of the slave QCL is at 485.8 mA (red), showing a non-linear phenomenon with quasi-regular pulsing and at 485.5 mA (blue), showing only noise. (b) Numerical simulation of the injection process displaying a periodic phenomenon close to the one observed experimentally. This result is obtained for an optical detuning of 1.2 GHz and a strong injection rate.

obtained by analyzing the light coming from the injected slave laser. But even if this value is centered around the frequency detuning, the RF spectrum is quite large, with a bandwidth of roughly 50 MHz. This led us to the conclusion that the non-linear pattern we observed is not a period-1 oscillation because its frequency spectrum is too complex. However, the limited bandwidth of the signal may not be in favor of chaos dynamics either, which is in agreement with a recent study pointing out that it could be difficult to generate chaos solely with optical injection in QCLs [137]. In other semiconductor lasers, the properties of the laser subject to injection varies a lot depending if it is considered as a highly-damped semiconductor laser [138] or not. In the case it is not, one can observe several dynamical behaviors [139] from chaos to period-1 and period-2 oscillations, with sometimes stability islands. In our case, the pattern keeps a steady RF spectrum signature whatever the injection-strength conditions and is visible from a near-zero detuning up to a detuning of 600 MHz, as can be seen in figure 11. The influence of the drive laser is strong for detuning values below 100 MHz and around 400 MHz. Apart from those values, the noise becomes predominant and limits the analysis of the slave signal. It is relevant to note that the frequency of the pattern is very sensitive to the emission properties of the slave QCL or the master QCL. For instance, if the bias current undergoes a 100 μA variation, this corresponds to a frequency detuning of 75 MHz and this modifies the frequency of the observed pattern. Even if not carefully assessed, a change in the heat sink temperature would lead to the same conclusion because the optical spectrum of a QCL is strongly dependent on the temperature of the structure.

5.3. Injection of giant pulses

As we previously saw, mid-IR QCLs are able to generate giant pulses and further tuning of the spiking is possible by adding an electrical excitation. However, the amplitude and the frequency of the excitation

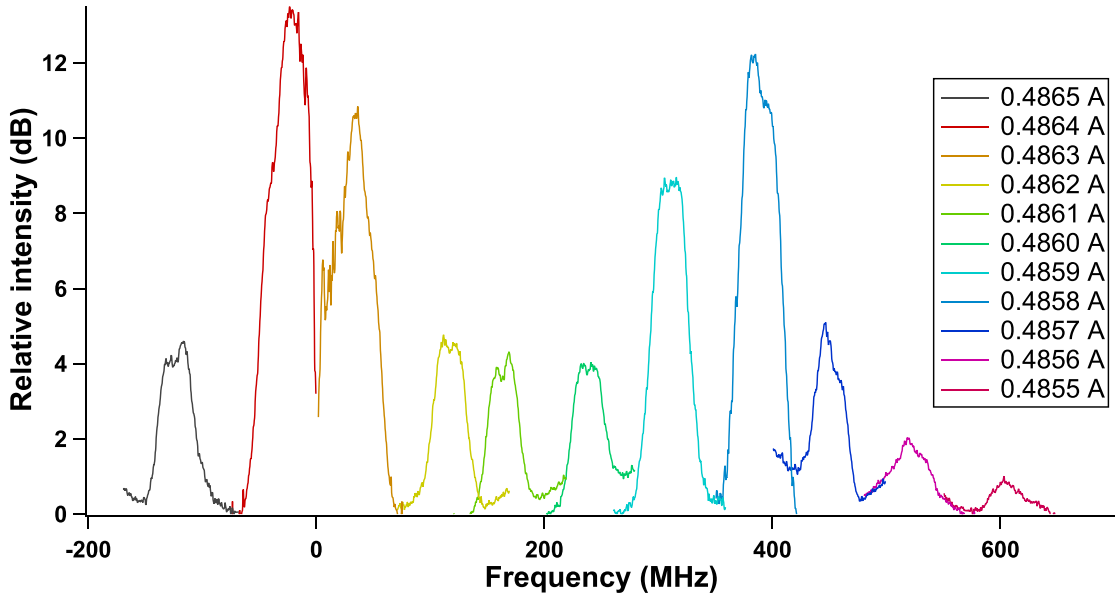

Figure 11. RF spectrum of the slave QCL when varying the pump current of the slave QCL and thus the frequency detuning between the two lasers. The peak frequency for each case corresponds to the frequency detuning between the master laser and the slave laser. The influence of the master is visible up to a detuning of 600 MHz. Negative frequencies are only for convenience for the reader, and correspond to their positive frequency counterparts. The noise level is arbitrarily fixed at 0 dB.

cannot be set randomly if one wants to trigger spikes similar to those relevant in neuromorphic configurations [140]. Figure 12(a) blue curve gives an example of a periodic excitation (marked with light blue arrows) that has no impact on the spiking dynamics of the QCL under study. Indeed, the QCL exhibit pulses with a consistent amplitude but these trains of pulses are made of an arbitrary number of spikes and the excitation does not give any indication about the upcoming sequence. To complement our study about injection in QCLs, we decide to unilaterally inject the spiking output of the master into the slave laser instead of injecting the signal of a free-running master QCL. Contrary to what is observed in the case of chaos synchronization [141] where the output of the slave laser reproduces the output of the master laser, we observe that the slave laser produces an optical signal that is close to the time derivative of the master's signal. Figure 12 shows the spiking master signal, the slave response signal and the numerical time derivative of the master's signal. One can see that the slave laser displays a response every time the master laser triggers a spike. A closer look at the slave's signal shows that the response (in red) is similar to the calculated time derivative (in black) and more specifically when the master's signal has a positive slope. In that specific case, the response of the slave displays a main pulse followed by weaker oscillations which are also found in the numerical calculation. When the master signal shows a decreasing slope, the slave laser outputs a magnified response compared to the numerical calculation, but the shape of the response is still consistent. We thus experimentally demonstrated an all-optical differentiator with an unilaterally injected QCL. The concept of differentiator, that is commonly used in electronics circuits [142], is relevant to perform all-optical edge detection [143, 144]. This achievement paves the way toward complex photonics at mid-IR wavelength and complements the recent experimental efforts about basic optical neurons in QCLs [145]. The explanation for the slave's behavior is the object of ongoing work but to the best of our knowledge, this differentiator feature has not yet been explored theoretically and experimentally in other semiconductor lasers such as laser diodes and VCSELs. This is worth noting because usually, the dynamics observed in QCLs have previously been thoroughly reported in near-infrared semiconductor lasers. Further experimental work will also consider the case of mutually coupled lasers without optical isolator in between [146]. In the case of QCLs, it was shown theoretically that this configuration also exhibits non-linear dynamics with a frequency centered around the optical detuning between the two lasers, provided that this detuning is far outside the locking range [147].

6. Toward secure applications with QCL's non-linear dynamics

Applications such as private communication based on chaos synchronization or physical random bit generation require complex chaos dynamics. In such chaos configuration, the attractor shows no discernible structure, indicating that the chaos can be highly dimensional, which is of paramount importance for

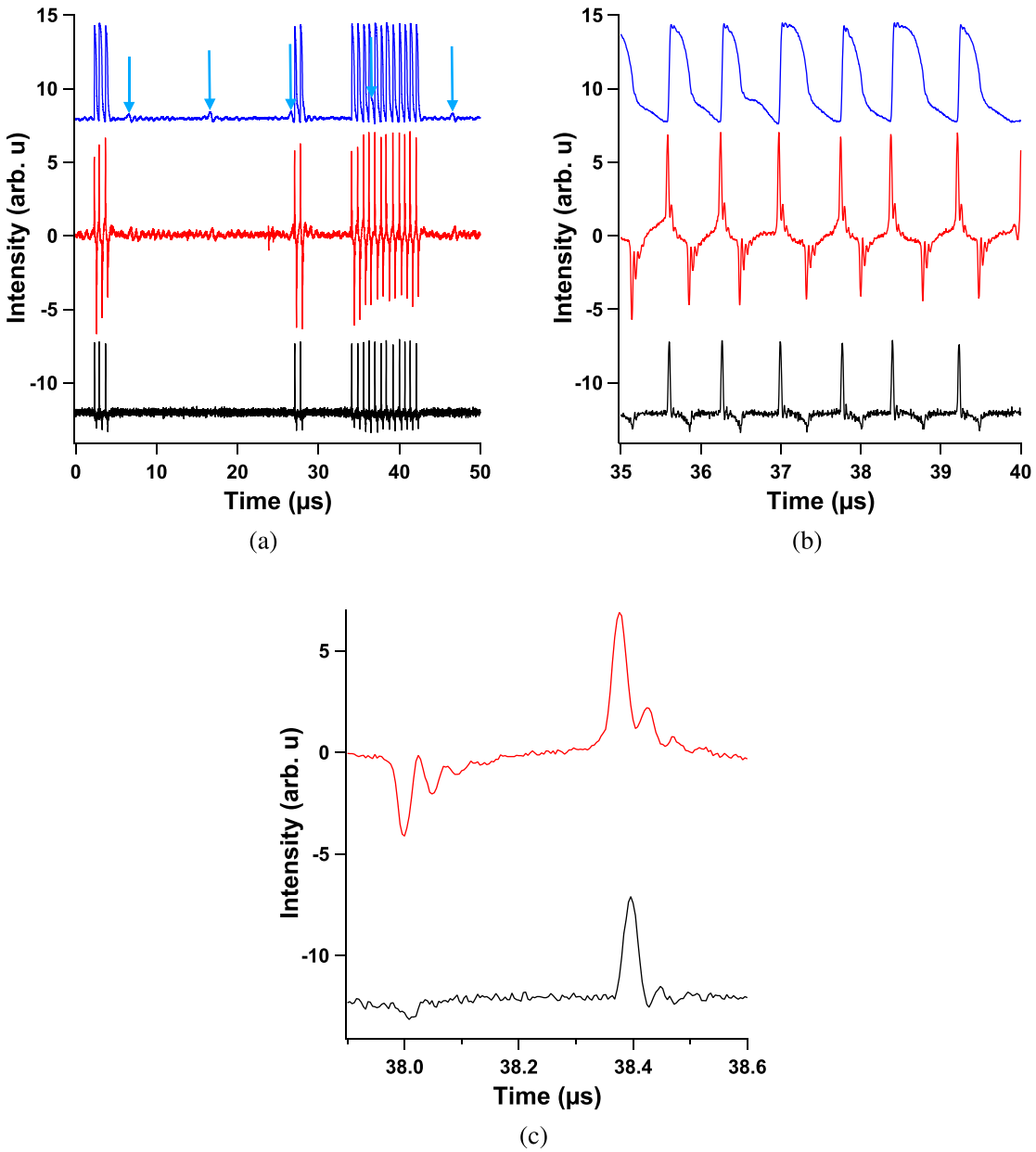

Figure 12. Experimental time traces of the output of the master QCL (blue), the injected slave QCL (red) and the calculated derivative of the master signal (black) when the master laser exhibits pulses which are not triggered by an electrical excitation; (a) global picture showing that the pulse-up excitation (light blue arrows) has no influence on the spiking dynamics of the master; (b) zoom on the behavior of the slave QCL when the master QCL fires a spike; (c) focus on the similarities between the slave's signal and the calculated derivative of the master's signal, the pulse-down occurs simultaneously in both cases but their amplitude is different while the pulse-up occurs also simultaneously with a comparable intensity.

increasing the privacy of the communication links and the data rate of the random bit stream. When studying private communication with chaos synchronization, a particular attention must be paid to the conditions of operation of the two lasers in order to limit any time-divergence. In the case of general synchronization [132], this may not be an issue since the synchronization area spreads around a wide bunch of parameters. But in the case of complete synchronization, which is more likely to happen for low rates of injection from the master laser to the slave laser, any shifting may be enough to stop the synchronization. The aforementioned method relying on synchronization is not the only way chaos can be utilized for private communication. Other methods of communication relying on chaos have been successfully tested through an accurate control over the emitted chaos fluctuations [148]. Control can be utilized to tune the signal emitted by the chaotic system so that it follows a prescribed symbol sequence, and this allows encoding any desired message from a chaotic oscillator. Most of the time, the phase diagram of such oscillators gathers multiple orbit attractors which are paired with a grammar [149]. The purpose is to choose a code whereby any message to be

transmitted can be encoded with a sequence included in the grammar. This sequence must bind a structure that is compatible with the constraints imposed by the dynamics in the presence of the control, which could be, for example, a periodic modulation. Therefore, it is of prime importance to control the spiking with thoroughness for reproducibility reasons and this can be achieved with drive-current modulation, external-cavity phase modulation or cavity-loss modulation [150], the perturbation being small compared to the chaos fluctuations [151]. However, as the phase space breaks up into distinct partitions [152], each of them corresponding to a distinct symbol, this solution is not necessarily the best in terms of privacy, even if efforts have already shown ways to improve it [153]. Nonetheless, this configuration is more prone to complete synchronization since the temperature of the device remains steady for small perturbations.

7. Conclusion

We have focused on the several non-linear dynamics QCLs can exhibit with a particular focus on EOF and optical injection. The former was found useful to display two kinds of chaos dynamics, namely LFFs and coherence-collapse regime. These non-linear phenomena are of utter interest for the realization of private communication based on chaos synchronization and for physical random number generation. When tilting the external cavity mirror, QCLs can exhibit giant pulses and further control of these pulses is possible via a pulse-up excitation with specific parameters. This concept is the cornerstone of neuromorphic photonics where semiconductor lasers reproduce the behavior of biological neurons to process complex tasks. The optical injection analysis displayed less complex dynamics in the output of the slave laser and this may be explained by the overdamped nature of QCLs. Nevertheless, when the drive signal is not in a free-running state but exhibits spiking dynamics, the slave QCL generates a signal close to the time derivative of the spiking pattern, which differs from regular chaos synchronization where the slave's output tends to be a copy of the master's output. This finding needs more investigation, especially on the numerical side, but accounts as a new tool for complex photonics with QCLs. More generally, for all the non-linear dynamics we exhibited in this article, as the technology of QCL is less mature than that for regular laser diodes and VCSELs, theoretical background is still sparse and will be required in the future to confront the experimental efforts.

Data availability statement

The data that support the plots within this paper and other findings of this study are available from the corresponding authors upon reasonable request.

Acknowledgments

This work is supported by the French Defense Agency (DGA), the French ANR program (ANR-17-ASMA-0006) and the European Office of Aerospace Research and Development (FA9550-18-1-7001). Authors thank Dr Andreas Herdt and Prof. Wolfgang Elsäßer for their initial help in the experimental efforts. The authors are grateful to mirSense for providing the quantum cascade oscillators.

Additional information

The authors declare no competing interests.

ORCID iDs

Olivier Spitz https://orcid.org/0000-0002-3868-5258
Frédéric Grillot https://orcid.org/0000-0001-8236-098X

References

[1] Faist J 2013 *Quantum Cascade Lasers* (Oxford: Oxford University Press)
[2] Vitiello M S, Scalari G, Williams B S and De Natale P 2015 *Opt. Express* **23** 5167–82
[3] Khalatpour A, Paulsen A K, Deimert C, Wasilewski Z R and Hu Q 2021 *Nat. Photon.* **15** 16–20
[4] Kapsalidis F, Schneider B, Singleton M, Bertrand M, Gini E, Beck M and Faist J 2021 *Appl. Phys. Lett.* **118** 071101
[5] Vitiello M S, Consolino L, Inguscio M and De Natale P 2021 *Nanophotonics* **10** 187–94
[6] Faist J, Capasso F, Sivco D L, Sirtori C, Hutchinson A L and Cho A Y 1994 *Science* **264** 553–6
[7] Lu Q, Slivken S, Wu D and Razeghi M 2020 *Opt. Express* **28** 15181–8
[8] Sobolev N and Sokovikov V V 1967 *Sov. Phys. Usp.* **10** 153
[9] Tacke M 1995 *Infrared Phys. Technol.* **36** 447–63

[10] Day T, Pushkarsky M, Caffey D, Cecchetti K, Arp R, Whitmore A, Henson M and Takeuchi E B 2013 Quantum cascade lasers for defense and security *Technologies for Optical Countermeasures X; and High-Power Lasers 2013: Technology and Systems* vol 8898 (Int. Society for Optics and Photonics) p 889802
[11] Bizet L, Vallon R, Parvitte B, Brun M, Maisons G, Carras M and Zeninari V 2017 *Appl. Phys.* B **123** 145
[12] Spitz O, Didier P, Durupt L, Díaz-Thomas D A, Baranov A N, Cerutti L and Grillot F 2021 *IEEE J. Sel. Top. Quantum Electron.* **28** 1–9
[13] Kuepper C, Kallenbach-Thieltges A, Juette H, Tannapfel A, Großerueschkamp F and Gerwert K 2018 *Sci. Rep.* **8** 1–10
[14] Isensee K, Kröger-Lui N and Petrich W 2018 *Analyst* **143** 5888–5911
[15] Vurgaftman I, Bewley W, Bartolo R, Felix C, Jurkovic M, Meyer J, Yang M, Lee H and Martinelli R 2000 *J. Appl. Phys.* **88** 6997–7005
[16] Smowton P M, Pearce E J, Schneider H, Chow W and Hopkinson M 2002 *Appl. Phys. Lett.* **81** 3251–3
[17] Grillot F, Dagens B, Provost J G, Su H and Lester L F 2008 *IEEE J. Quantum Electron.* **44** 946–51
[18] Maulini R, Yarekha D A, Bulliard J M, Giovannini M, Faist J and Gini E 2005 *Opt. Lett.* **30** 2584–6
[19] Henry C 1982 *IEEE J. Quantum Electron.* **18** 259–64
[20] Haken H 1970 Laser theory *Light and Matter Ic/Licht und Materie Ic* (Berlin: Springer) pp 1–304
[21] Elsässer W 1984 *Appl. Phys. Lett.* **44** 1126–8
[22] Vahala K and Yariv A 1983 *IEEE J. Quantum Electron.* **19** 1102–9
[23] Yariv A 1991 *Optical Electronics* (Philadelphia: Saunders College Publishing)
[24] Schawlow A L and Townes C H 1958 *Phys. Rev.* **112** 1940
[25] Osinski M and Buus J 1987 *IEEE J. Quantum Electron.* **23** 9–29
[26] Pereira M 2016 *Appl. Phys. Lett.* **109** 222102
[27] Hakki B W and Paoli T L 1975 *J. Appl. Phys.* **46** 1299–306
[28] Donati S 1978 *J. Appl. Phys.* **49** 495–7
[29] Aellen T, Maulini R, Terazzi R, Hoyler N, Giovannini M, Faist J, Blaser S and Hvozdara L 2006 *Appl. Phys. Lett.* **89** 091121
[30] Von Staden J, Gensty T, Elsäßer W, Giuliani G and Mann C 2006 *Opt. Lett.* **31** 2574–6
[31] Green R P, Xu J H, Mahler L, Tredicucci A, Beltram F, Giuliani G, Beere H E and Ritchie D A 2008 *Appl. Phys. Lett.* **92** 071106
[32] Spitz O, Herdt A, Duan J, Carras M, Elsäßer W and Grillot F 2019 Extensive study of the linewidth enhancement factor of a distributed feedback quantum cascade laser at ultra-low temperature *Quantum Sensing and Nano Electronics and Photonics XVI* vol 10926 (Int. Society for Optics and Photonics) p 1092619
[33] Lang R and Kobayashi K 1980 *IEEE J. Quantum Electron.* **16** 347–55
[34] Jumpertz L 2017 *Nonlinear Photonics in Mid-Infrared Quantum Cascade Lasers* (Berlin: Springer)
[35] Grillot F 2009 *IEEE J. Quantum Electron.* **45** 720–9
[36] Haken H 1975 *Phys. Lett.* A **53** 77–8
[37] Kimura T and Otsuka K 1970 *IEEE J. Quantum Electron.* **6** 764–9
[38] Van Tartwijk G H and Agrawal G P 1998 *Prog. Quantum Electron.* **22** 43–122
[39] Arecchi F, Lippi G, Puccioni G and Tredicce J 1984 *Opt. Commun.* **51** 308–14
[40] Strogatz S H 2018 *Nonlinear Dynamics and Chaos: With Applications to Physics, Biology, Chemistry and Engineering* (Boca Raton, FL: CRC Press)
[41] Weiss C, Abraham N and Hübner U 1988 *Phys. Rev. Lett.* **61** 1587
[42] Ohtsubo J 2012 *Semiconductor Lasers: Stability, Instability and Chaos* vol 111 (Berlin: Springer)
[43] Arecchi F, Meucci R, Puccioni G and Tredicce J 1982 *Phys. Rev. Lett.* **49** 1217
[44] Dangoisse D, Glorieux P and Hennequin D 1987 *Phys. Rev.* A **36** 4775
[45] Paiella R *et al* 2001 *Appl. Phys. Lett.* **79** 2526–8
[46] Agrawal G P and Dutta N K 2013 *Semiconductor Lasers* (Berlin: Springer Science & Business Media)
[47] Glas P, Müller R and Klehr A 1983 *Opt. Commun.* **47** 297–301
[48] Kikuchi K and Okoshi T 1982 *Electron. Lett.* **18** 10–12
[49] Agrawal G 1984 *IEEE J. Quantum Electron.* **20** 468–71
[50] Lin C, Burrus C and Coldren L 1984 *J. Lightwave Technol.* **2** 544–9
[51] Zhao B, Wang X and Wang C 2020 *ACS Photon.* **7** 1255–61
[52] Uchida A 2012 *Optical Communication with Chaotic Lasers: Applications of Nonlinear Dynamics and Synchronization* (New York: Wiley)
[53] Tkach R and Chraplyvy A 1986 *J. Lightwave Technol.* **4** 1655–61
[54] Kane D M and Shore K A 2005 *Unlocking Dynamical Diversity: Optical Feedback Effects on Semiconductor Lasers* (New York: Wiley)
[55] Donati S and Horng R H 2012 *IEEE J. Sel. Top. Quantum Electron.* **19** 1500309
[56] Jones R, Spencer P, Lawrence J and Kane D 2001 *IEEE Proc.-Optoelectron.* **148** 7–12
[57] Lenstra D, Verbeek B and Den Boef A 1985 *IEEE J. Quantum Electron.* **21** 674–9
[58] Azouigui S *et al* 2007 *Opt. Express* **15** 14155–62
[59] Sacher J, Elsäßer W and Göbel E O 1989 *Phys. Rev. Lett.* **63** 2224
[60] Chen C, Jia Z, Lv Y, Li P, Xu B and Wang Y 2021 *Opt. Lett.* **46** 5039–42
[61] Heil T, Fischer I and Elsäßer W 1998 *Phys. Rev.* A **58** R2672
[62] Pan M W, Shi B P and Gray G R 1997 *Opt. Lett.* **22** 166–8
[63] Mørk J, Mark J and Tromborg B 1990 *Phys. Rev. Lett.* **65** 1999
[64] Fischer I, Van Tartwijk G, Levine A, Elsässer W, Göbel E and Lenstra D 1996 *Phys. Rev. Lett.* **76** 220
[65] Sukow D W, Gardner J R and Gauthier D J 1997 *Phys. Rev.* A **56** R3370
[66] Torcini A, Barland S, Giacomelli G and Marin F 2006 *Phys. Rev.* A **74** 063801
[67] Jumpertz L, Schires K, Carras M, Sciamanna M and Grillot F 2016 *Light: Sci. Appl.* **5** e16088
[68] Mørk J, Tromborg B and Christiansen P L 1988 *IEEE J. Quantum Electron.* **24** 123–33
[69] Sacher J, Elsäßer W and Gobel E O 1991 *IEEE J. Quantum Electron.* **27** 373–9
[70] Mørk J, Tromborg B and Mark J 1992 *IEEE J. Quantum Electron.* **28** 93–108
[71] Fischer I, Hess O, Elsäßer W and Göbel E 1994 *Phys. Rev. Lett.* **73** 2188
[72] Brandstetter M and Lendl B 2012 *Sens. Actuators* B **170** 189–95
[73] Serebryakov V, Boĭko E, Kalintsev A, Kornev A, Narivonchik A and Pavlova A 2015 *J. Opt. Technol.* **82** 781–8

[74] Tholl H D 2018 Review and prospects of optical countermeasure technologies *Technologies for Optical Countermeasures XV* vol 10797 (Int. Society for Optics and Photonics) p 1079702
[75] Capasso F *et al* 2002 *IEEE J. Quantum Electron.* **38** 511–32
[76] Kumazaki N, Takagi Y, Ishihara M, Kasahara K, Sugiyama A, Akikusa N and Edamura T 2008 *Japan. J. Appl. Phys.* **47** 6320
[77] Hangauer A and Wysocki G 2015 *IEEE J. Sel. Top. Quantum Electron.* **21** 74–84
[78] Mezzapesa F, Columbo L, Brambilla M, Dabbicco M, Borri S, Vitiello M, Beere H, Ritchie D and Scamarcio G 2013 *Opt. Express* **21** 13748–57
[79] Spitz O, Herdt A, Wu J, Maisons G, Carras M, Wong C W, Elsäßer W and Grillot F 2021 *Nat. Commun.* **12** 1–8
[80] Shi B, Luo C, Flores J G F, Lo G, Kwong D L, Wu J and Wong C W 2020 *Opt. Express* **28** 36685–95
[81] Spitz O, Wu J, Herdt A, Carras M, Elsässer W, Wong C W and Grillot F 2019 *IEEE J. Sel. Top. Quantum Electron.* **25** 1–11
[82] Spitz O, Wu J, Carras M, Wong C W and Grillot F 2018 *Laser Phys. Lett.* **15** 116201
[83] Vicente R, Daudén J, Colet P and Toral R 2005 *IEEE J. Quantum Electron.* **41** 541–8
[84] Columbo L and Brambilla M 2014 *Opt. Express* **22** 10105–18
[85] Agrawal G P and Klaus J T 1991 *Opt. Lett.* **16** 1325–7
[86] Yariv A 1978 *IEEE J. Quantum Electron.* **14** 650–60
[87] Purcell E M 1977 *Am. J. Phys.* **45** 3–11
[88] Fink M 1992 *IEEE Trans. Ultrason. Ferroelectr. Freq. Control* **39** 555–66
[89] Cronin-Golomb M, Fischer B, White J O and Yariv A 1984 *IEEE J. Quantum Electron.* **20** 12–30
[90] Weicker L, Wolfersberger D and Sciamanna M 2018 *Phys. Rev.* E **98** 012214
[91] Uy C H, Weicker L, Rontani D and Sciamanna M 2018 *Opt. Express* **26** 16917–24
[92] Gavrielides A, Erneux T, Sukow D W, Burner G, McLachlan T, Miller J and Amonette J 2006 *Opt. Lett.* **31** 2006–8
[93] Takeuchi Y, Shogenji R and Ohtsubo J 2008 *Appl. Phys. Lett.* **93** 181105
[94] Heil T, Uchida A, Davis P and Aida T 2003 *Phys. Rev.* A **68** 033811
[95] Spitz O, Herdt A, Elsässer W and Grillot F 2021 *J. Opt. Soc. Am.* B **38** B35–9
[96] Donelan M A, Drennan W M and Magnusson A K 1996 *J. Phys. Oceanogr.* **26** 1901–14
[97] Onorato M *et al* 2009 *Phys. Rev. Lett.* **102** 114502
[98] Yan Z 2011 *Phys. Lett.* A **375** 4274–9
[99] Ganshin A, Efimov V, Kolmakov G, Mezhov-Deglin L and McClintock P V 2008 *Phys. Rev. Lett.* **101** 065303
[100] El-Labany S, Moslem W, El-Bedwehy N, Sabry R and El-Razek H A 2012 *Astrophys. Space Sci.* **338** 3–8
[101] Dean R 1990 Freak waves: a possible explanation *Water Wave Kinematics* (Berlin: Springer) pp 609–12
[102] Solli D, Ropers C, Koonath P and Jalali B 2007 *Nature* **450** 1054
[103] Dudley J M, Genty G, Mussot A, Chabchoub A and Dias F 2019 *Nat. Rev. Phys.* **1** 675–89
[104] Marcucci G, Pierangeli D and Conti C 2020 *Phys. Rev. Lett.* **125** 093901
[105] Bonatto C, Feyereisen M, Barland S, Giudici M, Masoller C, Leite J R R and Tredicce J R 2011 *Phys. Rev. Lett.* **107** 053901
[106] Schires K, Hurtado A, Henning I and Adams M 2012 *Electron. Lett.* **48** 872–4
[107] Ahuja J, Nalawade D B, Zamora-Munt J, Vilaseca R and Masoller C 2014 *Opt. Express* **22** 28377–82
[108] Alvarez N M, Borkar S and Masoller C 2017 *Eur. Phys. J. Spec. Top.* **226** 1971–7
[109] Reinoso J A, Zamora-Munt J and Masoller C 2013 *Phys. Rev.* E **87** 062913
[110] Choi D, Wishon M J, Barnoud J, Chang C, Bouazizi Y, Locquet A and Citrin D 2016 *Phys. Rev.* E **93** 042216
[111] Mercier E, Even A, Mirisola E, Wolfersberger D and Sciamanna M 2015 *Phys. Rev.* E **91** 042914
[112] Lee M W, Baladi F, Burie J R, Bettiati M A, Boudrioua A and Fischer A P 2016 *Opt. Lett.* **41** 4476–9
[113] Turconi M, Garbin B, Feyereisen M, Giudici M and Barland S 2013 *Phys. Rev.* E **88** 022923
[114] Perrone S, Vilaseca R, Zamora-Munt J and Masoller C 2014 *Phys. Rev.* A **89** 033804
[115] Hurtado A and Javaloyes J 2015 *Appl. Phys. Lett.* **107** 241103
[116] Jin T, Siyu C and Masoller C 2017 *Opt. Express* **25** 31326–36
[117] Lin S S, Hwang S K and Liu J M 2015 *Opt. Express* **23** 18256–68
[118] Hejda M, Robertson J, Bueno J and Hurtado A 2020 *J. Phys.: Photon.* **2** 044001
[119] Wang X G, Zhao B B, Deng Y, Kovanis V and Wang C 2021 *Phys. Rev.* A **103** 023528
[120] Residori S, Bortolozzo U, Montina A, Lenzini F and Arecchi F 2012 *Fluctuation Noise Lett.* **11** 1240014
[121] Karsaklian Dal Bosco A, Wolfersberger D and Sciamanna M 2013 *Opt. Lett.* **38** 703–5
[122] Erzgräber H, Lenstra D, Krauskopf B, Wille E, Peil M, Fischer I and Elsäßer W 2005 *Opt. Commun.* **255** 286–96
[123] Kobayashi S and Kimura T 1981 *IEEE J. Quantum Electron.* **17** 681–9
[124] Mogensen F, Olesen H and Jacobsen G 1985 *Electron. Lett.* **21** 696–7
[125] Spano P, Piazzolla S and Tamburrini M 1986 *IEEE J. Quantum Electron.* **22** 427–35
[126] Takiguchi Y, Ohyagi K and Ohtsubo J 2003 *Opt. Lett.* **28** 319–21
[127] Someya H, Oowada I, Okumura H, Kida T and Uchida A 2009 *Opt. Express* **17** 19536–43
[128] Taubman M S, Myers T L, Cannon B D and Williams R M 2004 *Spectrochim. Acta* A **60** 3457–68
[129] Simos H, Bogris A, Syvridis D and Elsäßer W 2013 *IEEE J. Quantum Electron.* **50** 98–105
[130] Juretzka C, Simos H, Bogris A, Syvridis D, Elsäßer W and Carras M 2014 *IEEE J. Quantum Electron.* **51** 1–8
[131] Borri S *et al* 2012 *Opt. Lett.* **37** 1011–13
[132] Ohtsubo J 2002 *IEEE J. Quantum Electron.* **38** 1141–54
[133] Meng B and Wang Q J 2012 *Opt. Express* **20** 1450–64
[134] Wang C, Grillot F, Kovanis V I, Bodyfelt J D and Even J 2013 *Opt. Lett.* **38** 1975–7
[135] Wang C, Grillot F, Kovanis V and Even J 2013 *J. Appl. Phys.* **113** 063104
[136] Erneux T, Kovanis V and Gavrielides A 2013 *Phys. Rev.* E **88** 032907
[137] Zhao B B, Kovanis V and Wang C 2019 *IEEE J. Sel. Top. Quantum Electron.* **25** 1–7
[138] Hurtado A, Mee J, Nami M, Henning I D, Adams M J and Lester L F 2013 *Opt. Express* **21** 10772–8
[139] Simpson T, Liu J, Huang K and Tai K 1997 *Quantum Semiclass. Opt.: J. Eur. Opt. Soc.* B **9** 765
[140] Izhikevich E M 2003 *IEEE Trans. Neural Netw.* **14** 1569–72
[141] Fujino H and Ohtsubo J 2000 *Opt. Lett.* **25** 625–7
[142] Biswas K, Sen S and Dutta P K 2006 *IEEE Trans. Circ. Syst. II: Express Briefs* **53** 802–6
[143] Canny J 1986 *IEEE Trans. on Pattern Analysis and Machine Intelligence* pp 679–98
[144] Robertson J, Zhang Y, Hejda M, Bueno J, Xiang S and Hurtado A 2020 *Opt. Express* **28** 37526–37

[145] Spitz O, Wu J, Herdt A, Maisons G, Carras M, Elsäßer W, Wong C W and Grillot F 2020 *Adv. Photon.* **2** 066001
[146] Erzgräber H, Wille E, Krauskopf B and Fischer I 2009 *Nonlinearity* **22** 585
[147] Herdt A, Weidmann M, Mohr T, Lenstra D and Elsäßer W 2018 Theory of delay-coupled nonidentical quantum cascade lasers *Semiconductor Lasers and Laser Dynamics VIII* vol 10682 (Int. Society for Optics and Photonics) p 106820H
[148] Hayes S, Grebogi C and Ott E 1993 *Phys. Rev. Lett.* **70** 3031
[149] Bollt E, Lai Y C and Grebogi C 1997 *Phys. Rev. Lett.* **79** 3787
[150] Naumenko A, Loiko N, Turovets S, Spencer P and Shore K 1998 *J. Opt. Soc. Am.* B **15** 551–61
[151] Shinbrot T, Grebogi C, Yorke J A and Ott E 1993 *Nature* **363** 411
[152] Sukow D W and Gauthier D J 2000 *IEEE J. Quantum Electron.* **36** 175–83
[153] Abel A and Schwarz W 2002 *Proc. IEEE* **90** 691–710